Article

Comparative Analysis of Instrumental and Manual Visibility Observations at Xiamen Airport and the Influence of Relative Humidity

Hangdong Jiang [1], Fei Li [2], Xiaohui Ren [3], Kaiwen Hu [1], Zhen Chen [1], Zhonghong Luo [1] and Pak Wai Chan [4,*]

[1] Xiamen Air Traffic Management Station, CAAC, Xiamen 361017, China; xmbirdwatcher@aliyun.com (H.J.); 18350214720@163.com (K.H.); townczzz@163.com (Z.C.); luobirdwatcher@126.com (Z.L.)
[2] Xiamen Key Laboratory of Straits Meteorology, Xiamen Meteorological Bureau, Xiamen 361012, China; leefeicat@163.com
[3] Aviation Meteorological Center, Air Traffic Management Bureau, CAAC, Beijing 100122, China; renxiaohui@atmb.net.cn
[4] Hong Kong Observatory, Hong Kong 999077, China
* Correspondence: pwchan@hko.gov.hk

Abstract: Visibility is a major factor affecting the safety and efficiency of aviation operations. As instrumental visibility measurements are the basis for calculating runway visual range, measurement accuracy is crucial. In this study, we collected instrumental visibility data (V_I) from two sets of Vaisala transmissometers (referred to as LT_{05} and LT_{23}) and one set of forward-scatter meters (referred to as FD) installed at Xiamen Airport. We also considered manually observed visibility (V_M) and relative humidity (RH) records of automatic weather stations for 2015 to 2020. Taking the V_M data as the benchmark, we comprehensively evaluated the difference between the V_I of each instrument and V_M as well as the influence of RH on such deviations based on the deviation (ΔV), relative deviation (ΔV_{Mdi}), root mean square error (RMSE), relative-RMSE, mean value, and correlation analysis method. Our results showed that: (1) among the three sets of visibility meters, the V_I values of LT_{05} were the closest to the V_M values under different V_M levels and at high RH. Deviations in the FD measurements were greater than those of the two LT sets under low-visibility conditions that significantly affect aviation operations ($V_M < 800$ m). (2) In general, the V_I values were lower than the V_M values, and the larger the V_M value, the greater the deviation. (3) Extremely large ΔV and ΔV_{Mdi} values appeared in spring when the visibility level was rapidly increasing or decreasing. (4) The FD results were greatly affected by RH, with higher proportions of large ΔV and large ΔV_{Mdi} data than the two LT sets under high-humidity conditions. Therefore, the Vaisala transmissometers outperformed the forward-scatter meter at the airports along the southeastern coast of China and those in high-humidity environments.

Keywords: visibility; deviation; transmissometer; forward-scatter meter; manual observation

1. Introduction

Visibility manifests a visual obstruction phenomenon and is a basic meteorological parameter. It is widely applied in transportation, meteorology, ecological conservation, and environmental protection. Runway visual range (RVR) is an essential meteorological indicator in the minimum standards set for airport operations [1], directly affecting the safety and efficiency of aviation operations [2]. Article 37 of the Technical Specification for Automatic Meteorological Observation System for Civil Aviation (AP-117-TM-2018-03R1, Civic Aviation Administration of China, Beijing, China) issued by the Civil Aviation Administration of China sets strict requirements for the accuracy of visibility meters. When the meteorological optical range (MOR) measured using a visibility meter is less than or equal to 600 m, the maximum permissible error is 50 m. When 600 m < MOR ≤ 1500 m,

the maximum permissible error is 10% of the MOR. When MOR > 1500 m, the maximum permissible error is 20% of the MOR. Hence, accurate visibility observations are crucial for aviation safety.

Before the 1990s, visibility data from airports in China were obtained entirely by manual observation. With the deployment and operation of the automatic weather observation system (AWOS) at Beijing Capital International Airport in 1985 [3], visibility measurements started to be performed both automatically and manually at China's airports, and real-time, objective, and high-temporal-resolution monitoring of visibility at airport runways has already been realised. However, due to differences in the measurement principles and detection ranges between visibility meters and manual observation methods [4], the visibility values in the meteorological aerodrome reports (METAR) provided by airports are still those obtained through manual observation.

The available visibility meters can be divided into transmissometers and scatter meters according to their measurement principles [5]. They are all designed based on Koschmieder and Allard's law, but the detection methods differ [6–9], with different sources of error [10–12]. Researchers have conducted many comparison experiments, assessments, and calibrations to reduce the errors of these two types of visibility meters [13–20]. Meanwhile, many scholars have compared the instrument-observed visibility values with those obtained through manual observation to apply the instrumental measurements rationally [21–25]. Some studies have focused on the differences between the records of several visibility meters of the same type and the manual observations within specific regions, and others have analysed the differences between the visibility values obtained using multiple sets of instruments of the same type and the manual observations obtained at the same site. However, most of these studies performed qualitative statistical analyses of correlation results and deviation trends. Data on manual observations available for comparative analysis are limited, and studies comparing instrumental and manual visibility observations at airports are scarce. Zhang et al. calculated the average absolute deviation between visibility values obtained from an FD12P forward-scatter(VAISALA, Vanta, Finland) meter at Guangzhou New Airport and those obtained through manual observation and comparatively analysed their differences under different visibility levels and low cloud cover [26]. He et al. used visibility data obtained using a DNQ1/V35 forward-scatter(Huayun Shengda (Beijing) Meteorological Technology Co., Ltd., Beijing, China) meter during the site selection stage for Ezhou international logistics core hub airport as well as visibility data obtained through manual observation during the daytime to analyse the differences between the two by calculating the mean and standard deviation of the difference between them [27]. In particular, there is a lack of quantitative analyses on the differences between the measurements of multiple types of visibility meters and the manual observations obtained at the same location. Transmissometers or forward-scatter visibility meters are currently installed at most airports in China. The application of instrument-measured visibility in aviation operations is becoming increasingly extensive, and there is an urgent need for a scientific basis for selecting suitable visibility meters during the construction of new airports. Therefore, it is necessary to evaluate the performance of different types of visibility meters and compare the differences between instrumental and manual visibility observations at Xiamen Airport.

In this study, we used the records of transmissometers and a forward-scatter visibility meter, as well as visibility measurements obtained through manual observation during the same period at Xiamen Airport from 2015 to 2020, to compare the data collected using different types of visibility meters with those obtained through manual observation. We analysed the distribution of the difference between the instrumental and manual results and the possible reasons and also assessed the performance of different types of visibility meters under the influence of relative humidity (RH), aiming to provide technical support for reasonably planning the deployment of visibility meters at airports.

2. Materials and Methods

2.1. Study Area and Data Sources

The datasets used in this study include the hourly meteorological optical range (V_I) and RH collected by the AWOS at Xiamen Airport from January 2015 to December 2020 and the hourly data of manually observed visibility (V_M) and RH from METAR for the same period. The AWOS is equipped with two sets of the Vaisala double-ended transmissometers of model LT31 (referred to as LT) with a baseline length of 30 m as well as one set of forward-scatter visibility meters of model FD12P (referred to as FD) with a scattering angle of 33°. LT was used to measure the atmospheric transmissivity between the transmitter and receiver to obtain the mean extinction coefficient to evaluate visibility value V_I. Meanwhile, FD was used to evaluate the energy of near-infrared light with a forward-scatter angle of 33° caused by various suspended particles in the volume of air sampled, which was compared to the total light scattering to determine the total scattering coefficient. Thereafter, the extinction coefficient was derived, and visibility value V_I was inverted. According to civil aviation regulations [28,29], these instruments were installed on the northern side of the runway, 80–100 m from the runway centreline. The two sets of LT (referred to as LT_{05} and LT_{23}) were deployed at the two ends of the runway approximately 500 m inward, and FD was installed at the midpoint of the runway (see Figure 1). LT and FD are continuously monitored and regularly maintained. The field equipment is maintained weekly, and visibility calibration is performed monthly. The data processing software has an automatic alerting function so that engineers can be immediately notified to check data effectiveness in case of anomalies. Thus, the output data are of high quality. After eliminating abnormal data during brief equipment shutdowns required for maintenance, sensor coverage by foreign objects, or instrument damage due to typhoons, a valid V_I dataset consisting of 52,368 hourly time points was obtained.

Figure 1. Locations of the three sets of visibility meters in relation to the manual observation platform. The performance parameters of the three sets of visibility meters are as described in Table 1.

Table 1. Performance parameters of LT transmissometer and FD forward scatter meter.

Instrument Model	Measurement Range	Accuracy	Temporal Resolution	Baseline Length or Scattering Angle	Operating Environment
LT	10–10,000 m	±10%	1 min	30 m	−40 ± 60 °C RH: 0–100%
FD	10–15,000 m	±10%	1 min	33°	−40 ± 50 °C RH: 0–100%

V_M is the maximum horizontal distance visible throughout at least half of the horizon, not necessarily continuously [30]. It was determined by an observer at the manual observation platform using visual reference targets (target lamps) (see Figure 2). V_M provided services in the form of METAR messages. There were six to eight meteorological observation personnel issuing V_M messages at Xiamen Airport, and two to three people were arranged in rotation daily. The V_M value was generally published once daily. The

manual observation platform was on the northern side of the end of runway 05, with LT_{05} located approximately 120 m to its east, LT_{23} approximately 2500 m to its northeast, and FD approximately 1400 m to its northeast (see Figure 1). LT_{05} was the closest to the manual observation platform, followed by FD and then LT_{23}. Moreover, as per regulations, (1) when $V_M < 800$ m, the V_M value should be reported in increments of 50 m; (2) when 800 m $\leq V_M < 5000$ m, the V_M value should be reported in increments of 100 m; (3) when 5000 m $\leq V_M < 10,000$ m, the V_M value should be reported in increments of 1000 m; (4) if an observation does not fulfil the corresponding reporting requirement, the V_M value should be rounded off to the nearest level; and (5) when $V_M \geq 10,000$ m, the V_M value should be recorded as 9999 [29]. Thus, we processed all V_I data according to these criteria and eliminated the data corresponding to the time points with a V_M of 9999, obtaining a valid dataset consisting of 14,349 hourly time points. Moreover, since the upper detection limit of LT was 10,000 m, all FD data greater than 10,000 m were set to 10,000 m.
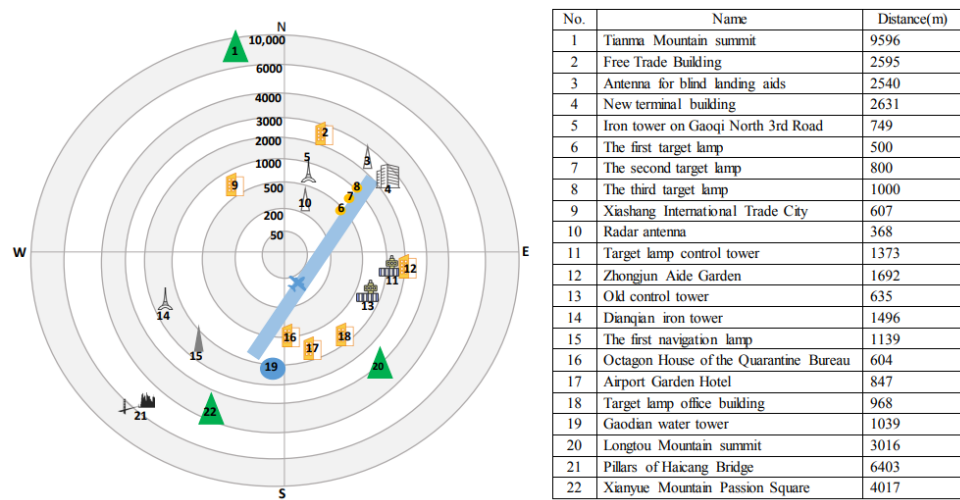

No.	Name	Distance(m)
1	Tianma Mountain summit	9596
2	Free Trade Building	2595
3	Antenna for blind landing aids	2540
4	New terminal building	2631
5	Iron tower on Gaoqi North 3rd Road	749
6	The first target lamp	500
7	The second target lamp	800
8	The third target lamp	1000
9	Xiashang International Trade City	607
10	Radar antenna	368
11	Target lamp control tower	1373
12	Zhongjun Aide Garden	1692
13	Old control tower	635
14	Dianqian iron tower	1496
15	The first navigation lamp	1139
16	Octagon House of the Quarantine Bureau	604
17	Airport Garden Hotel	847
18	Target lamp office building	968
19	Gaodian water tower	1039
20	Longtou Mountain summit	3016
21	Pillars of Haicang Bridge	6403
22	Xianyue Mountain Passion Square	4017

Figure 2. Distribution of visibility reference targets around Xiamen Airport.

The distance between the reference targets (target lamps) and the manual observation platform was determined by professional staff using precision instruments to approximate the true value of visibility. Therefore, the V_M levels were graded according to the distribution range of these reference targets. As shown in Figure 2, 10 targets (lamps) in four groups were distributed on almost the same distance contour; thus, we categorised V_M into the following eight levels after merging the adjacent targets (lamps): (1) $V_M \leq 368$ m; (2) 368 m $< V_M \leq 847$ m; (3) 847 m $< V_M \leq 1692$ m; (4) 1692 m $< V_M \leq 2539$ m; (5) 2539 m $< V_M \leq 3016$ m; (6) 3016 m $< V_M \leq 4017$ m; (7) 4017 m $< V_M \leq 6403$ m; and (8) 6403 m $< V_M \leq 9595$ m. The sample size in each interval is shown in Table 2. Table 2 lists the sample numbers of each visibility classification shown in Figures 3–6, and Table 3 lists the sample numbers of the RH classification shown in Figures 7–9.

Table 2. Distribution of V_I sample size in different V_M intervals (unit: hourly time points).

1	2	3	4	5	6	7	8	Total
40	29	201	603	626	1531	4599	6720	14,349

Table 3. Distribution of V_I sample size in different RH intervals (unit: hourly time points).

RH Level	1	2	3	4	5	6	7	Total
LT_{05}	75	214	746	1745	2890	4944	3735	14,349
FD	41	166	668	1532	2775	5093	4074	14,349
LT_{23}	21	127	554	1378	2662	4689	4918	14,349
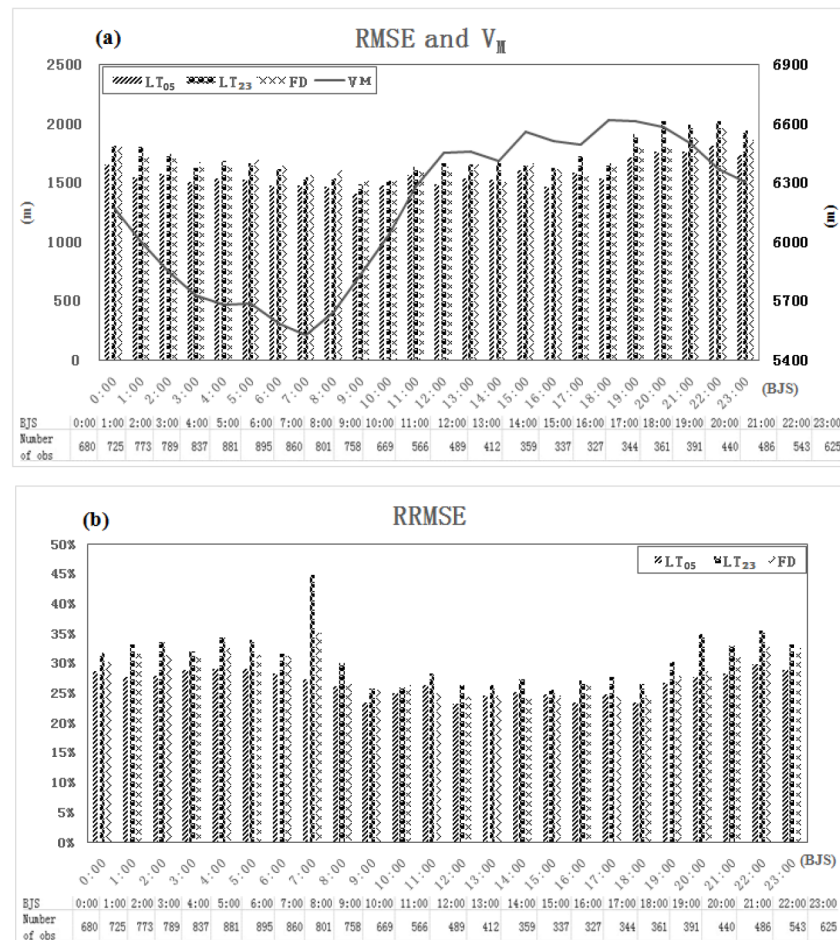
Figure 3. Daily variations of RMSE and RRMSE ((**a**): RMSE, (**b**): RRMSE).
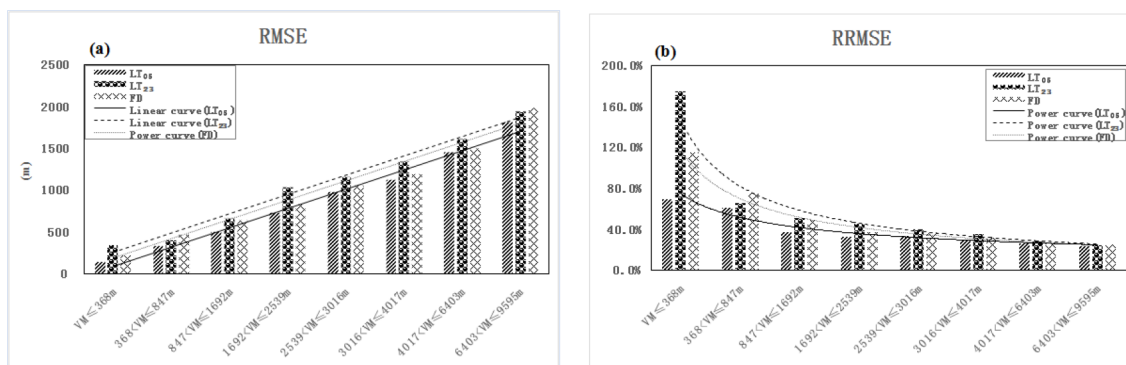

Figure 4. (**a**) RMSE and (**b**) RRMSE under different V_M levels from 2015 to 2020.
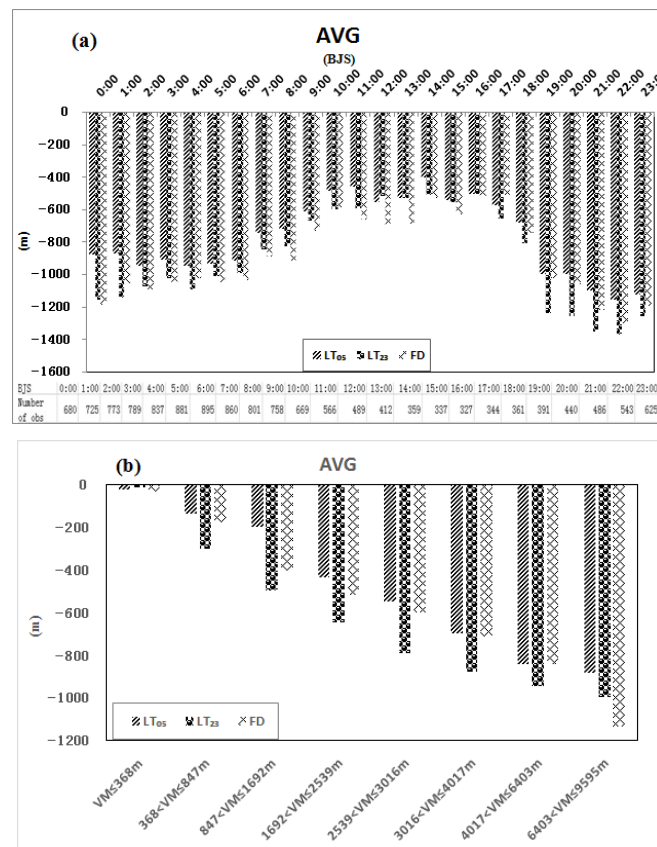
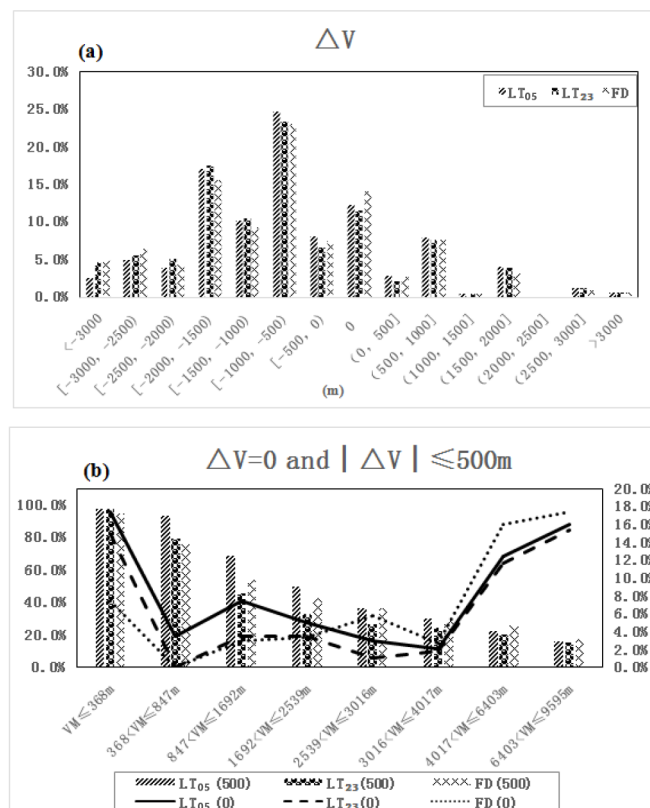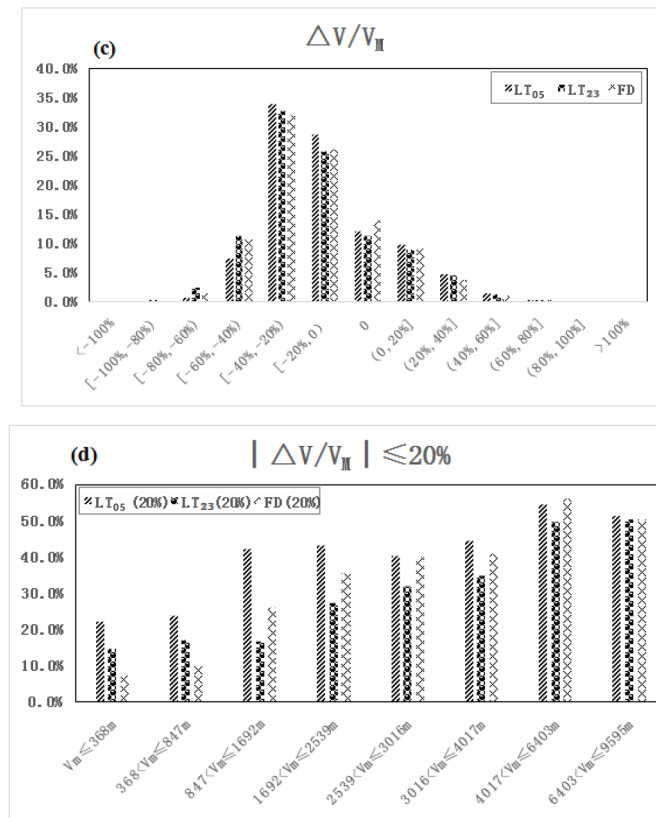**Figure 5.** Daily AVG variation of ΔV from 2015 to 2020 (**a**) and AVG of ΔV under various V$_M$ values (**b**).

Figure 6. *Cont.*

Figure 6. Proportional distributions of ΔV and ΔV_{Mdi} for the three visibility meters from 2015 to 2020 (**a**): ΔV; (**b**): ΔV = 0 and |ΔV| ≤ 500 m; (**c**): ΔV_{Mdi}; (**d**): |ΔV_{Mdi}| ≤ 20%).
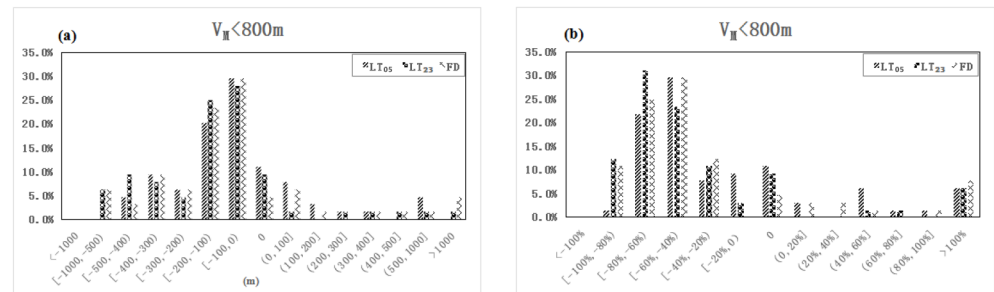
Figure 7. Proportional distributions of (**a**) ΔV and (**b**) ΔV_{Mdi} for the three visibility meters at V_{M800} from 2015 to 2020.
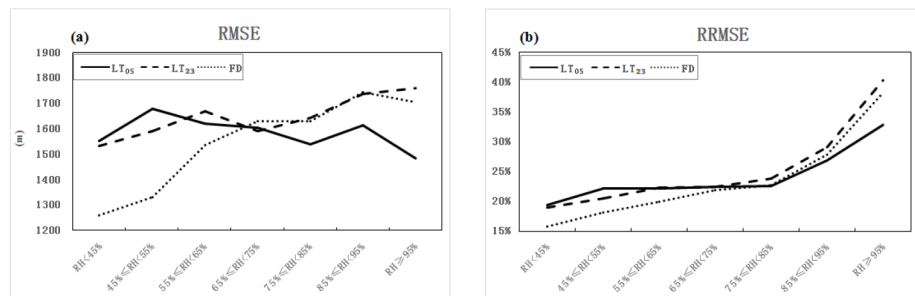

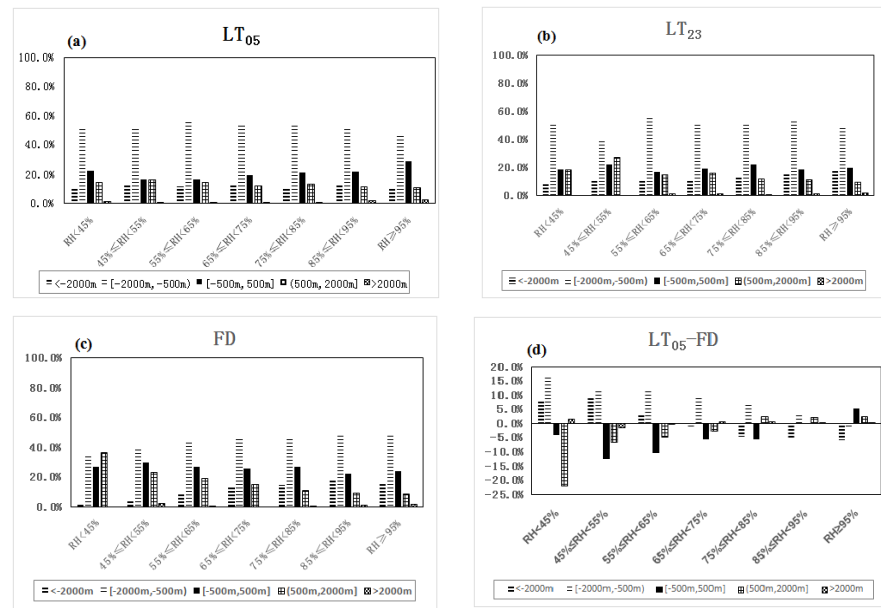**Figure 8.** Distributions of (**a**) RMSE and (**b**) RRMSE under different RH levels from 2015 to 2020.

Figure 9. Proportional distributions of (**a**) ΔV_{LT05}, (**b**) ΔV_{LT23}, (**c**) ΔV_{FD}, and (**d**) $\Delta V_{LT05\text{-}FD}$ under different RH levels from 2015 to 2020.

As Xiamen Airport is located near the sea, where the RH is high all year round, data corresponding to RH < 35% only accounted for 0.08% of the effective sample size. Therefore, we graded the RH values into the following seven levels: (1) RH < 45%; (2) 45% ≤ RH < 55%; (3) 55% ≤ RH < 65%; (4) 65% ≤ RH < 75%; (5) 75% ≤ RH < 85%; (6) 85% ≤ RH < 95%; and (7) RH ≥ 95%. The RH gauges were installed in the automatic weather stations near LT_{05} and LT_{23}, and the RH values in the METAR messages were taken from the instrument near LT_{05}. The RH values for FD were the averages of the records of the RH gauges near LT_{05} and LT_{23}. The distribution of the V_I sample size against RH is shown in Table 3.

2.2. Statistical Methods

Based on statistical principles, we calculated the agreement rate and gross error rate of the data and conducted correlation analyses. V_I and V_M were compared according to the data's deviation, relative deviation, root mean square error (RMSE), and mean. The meanings of the above statistics are explained below.

(1) Agreement rate: the V_I and V_M values were considered to be in agreement if the absolute value of the difference between them was less than or equal to two times the standard deviation of the difference [31]. The ratio of the cumulative number of agreements between V_I and V_M to the total number of valid observations was the agreement rate of the two visibility datasets, which reflected the consistency between V_I and V_M.

(2) Gross error rate: the difference between V_I and V_M was considered a gross error if its absolute value was greater than three times the standard deviation of the difference. The largest gross error value was then eliminated, the standard deviation of the difference between V_I and V_M was recalculated, and the difference values were filtered again according to the definition of the gross error to eliminate the largest one. The above steps were repeated until no difference values were considered gross errors. At this point, the number of gross error values eliminated was defined as the number of gross errors [31], and the ratio of the number of gross errors to the total number of effective observations was the gross error rate, which reflected the pattern of outliers in the difference between V_I and V_M.

(3) Deviation (ΔV): the difference of V_I minus V_M. The formula for calculating ΔV is $\Delta V = V_I - V_M$.

(4) Relative deviation (ΔV_{Mdi}): the ratio of ΔV to V_M. The formula for calculating ΔV_{Mdi} is $\Delta V_{Mdi} = \Delta V / V_M$.

(5) Root mean square error (RMSE): the square root of the mean of ΔV squared, reflecting the absolute deviation of V_I from V_M. The smaller the RMSE, the smaller the ΔV. The calculation formula is as shown in Equation (1).

$$\text{RMSE} = \sqrt{\frac{1}{n}\sum_{i=1}^{n}(V_{Ii} - V_{Mi})^2} \tag{1}$$

where n is the sample size, V_{Ii} is the V_I value at the i-th time point, and V_{Mi} is the V_M value at the i-th time point.

(6) Relative root mean square error (RRMSE): the square root of the mean of ΔV_{Mdi} squared, reflecting the relative deviation of V_I and V_M. The smaller the RRMSE, the smaller the degree of V_I's deviation relative to V_M. The calculation formula is as shown in Equation (2).

$$\text{RRMSE} = \sqrt{\frac{1}{n}\sum_{i=1}^{n}((V_{Ii} - V_{Mi})/V_{Mi})^2} \tag{2}$$

where n is the sample size, V_{Ii} is the V_I value at the i-th time point, and V_{Mi} is the V_M value at the i-th time point.

(7) The correlation coefficient *r* represents the correlation degree between V_I and V_M. The larger the r value, the stronger the correlation. The formula is:

$$r = \frac{\sum_1^n (V_{Ii} - \overline{V_I})(V_{Mi} - \overline{V_M})}{\sqrt{\sum_1^n (V_{Ii} - \overline{V_I})^2 \sum_1^n (V_{Mi} - \overline{V_M})^2}} \tag{3}$$

where n is the number of sample data, V_{Ii} is the value of V_I at time i, and V_{Mi} is the value of V_M at time i.

3. Results

3.1. Agreement and Correlation between V_I and V_M

The agreement rate, gross error rate, and correlation coefficient between V_I and V_M for each visibility meter are listed in Table 4. It can be seen that the agreement rate between V_I and V_M was high for all three sets of visibility meters, reaching approximately 90%. The V_I of these instruments was highly correlated with V_M, with correlation coefficients exceeding 0.8. The correlation coefficient between the V_I of LT and V_M was significantly higher than that between the V_I of FD and V_M; however, the gross error rate for LT was also considerably higher than that for FD, which may have been associated with the significantly higher standard deviation of the difference between V_I and V_M for FD than that for LT.

Table 4. Agreement rate, gross error rate, and correlation coefficient between V_I and V_M.

Visibility Meter	LT$_{05}$	LT$_{23}$	FD
Agreement rate	88.1%	93.2%	91.7%
Gross error rate	6.4%	7.6%	3.6%
Correlation coefficient	0.92	0.92	0.80

3.2. RMSE and RRMSE of V_I Relative to V_M

3.2.1. Daily Variation Characteristics of RMSE and RRMSE

As can be seen from Figure 3, the daily variation distributions of the RMSE (Figure 3a) and RRMSE (Figure 3b) of the three visibility meters were both large at night and small at day. They gradually increased at night, reached the highest value before midnight, gradually decreased in the early morning, and reached a minimum in the forenoon. This indicated that the difference between V_I and V_M was greater at night than during daytime, was the largest at midnight, and the smallest in the forenoon. This may be related to the fact that the number of target lamps at night was much less than the number of target

objects during the daytime (Figure 2). Manual observation of visibility at night is more subjective, and the V_M values obtained from different observers may vary greatly. Adding target lamps at night will effectively reduce the difference. In addition, Xiamen Airport is located in the north-eastern corner of Xiamen Island. Except for the north-eastern end facing the sea, the other three sides are surrounded by urban buildings. At night, city lights increase the brightness of the background, which reduces the brightness contrast of the target lamps, thereby affecting the observation results of the observer. When the lights are on at night, the difference between V_I and V_M increases, but after midnight, as the city lights decrease, the difference between V_I and V_M decreases.

Among the three visibility meters, the RMSE and RRMSE of LT_{05} were the smallest at all times, indicating the smallest difference between the V_I and V_M of LT_{05}. The RMSEs and RRMSEs of LT_{23} were similar to those of FD. In most cases, the LT_{23} values were slightly higher than those of FD and were significantly higher between 19:00 and 21:00. Notably, from 5:00 to 9:00, the RMSE of FD was higher than that of LT_{23}, which was the largest of the three, while the V_M of Xiamen Airport was the lowest at this time (Figure 3a). The RRMSE of LT_{23} was abnormally large at 07:00 and 20:00. This may have been because LT_{23} was installed on the coastal side, which makes it greatly affected by the air current over the sea. Thus, its V_I value fluctuates more than those of LT_{05} and FD installed inland.

In conclusion, anthropogenic causes increase the difference between V_I and V_M at night. The deviation and relative deviation of LT_{05} are the smallest at all times of the day. In the early morning, when V_M is in a trough, the difference between the V_I and V_M of the forward-scatter meter is greater than that of the atmospheric transmissometer.

3.2.2. Distribution Characteristics of RMSE and RRMSE at Different Visibility Levels

As shown in Figure 3a, the RMSE of V_I relative to V_M increased with increasing V_M for all three visibility meters, exhibiting a linear relationship ($R^2 > 0.97$). This means that the larger the V_M, the greater the ΔV. The ΔV of LT_{05} was the smallest at each V_M level; the ΔV of FD was the largest when 368 m $< V_M \leq$ 847 m and 6403 m $< V_M \leq$ 9595 m; the ΔV of LT_{23} was the largest when $V_M \leq$ 368 m and 847 m $< V_M \leq$ 6403 m. Xiamen Airport is located near the sea, where the visibility level has significant spatial–temporal variations. Runway 23 was constructed on land reclaimed from the sea and frequently affected by sea fog; therefore, the visibility at the end of runway 23 is generally lower than that at other localities. Thus, the ΔV of LT_{23} was especially large at a low V_M. In contrast, the ΔV of FD was higher than those of the two sets of LT at a high V_M (>6403 m) due to the limitations of the forward-scatter meter's detection principle. Consistent with relevant results, the scattering error increased at high visibility [32,33]. In addition, at V_{M800} ($V_M <$ 800 m, the same below), which has a crucial impact on aviation operations, the ΔV of FD was also greater than those of the two sets of LT when the visibility was at approximately the minimum operating standards for Xiamen Airport (RVR > 400 m for take-off and RVR > 550 m for landing; 368 m $< V_M \leq$ 847 m).

The RRMSE of V_I relative to V_M exhibited a power relationship with V_M ($R^2 > 0.96$) for all of the instruments (see Figure 3b). As V_M increased, RRMSE decreased rapidly; when $V_M >$ 1692 m, the decreasing curves started to level off, with a difference in RRMSE between adjacent V_M levels of less than 6%; when $V_M >$ 3016 m, the RRMSE of each instrument was consistent. The RRMSE of LT_{05} was the smallest at each V_M level; the RRMSE of LT_{23} was the largest when $V_M \leq$ 368 m and 847 m $< V_M \leq$ 3016 m; and the RRMSE of FD was the largest when 368 m $< V_M \leq$ 847 m.

From the above analysis, we can infer that, among the three sets of visibility meters, the V_I of LT_{05} was the closest to V_M at each V_M level. At V_{M800}, when $V_M \leq$ 368 m, the deviation of V_I from V_M was the most significant for LT_{23}; when $V_M >$ 368 m, the deviation was the greatest for FD.

3.3. Mean Values of V_I's Deviation Relative to V_M

The mean values of ΔV, the difference between the V_I and V_M of the three visibility meters, were negative at all times (Figure 5a), and its absolute value at night was greater than that during the day. The absolute value was the lowest at noon, gradually increasing in the evening and reaching a maximum before midnight. The absolute value of LT_{05} was always the smallest. LT23 had the largest absolute value between evening and midnight, and FD had the largest absolute value at other times. This indicates that, on average, the difference between V_I and V_M was greater at night than during the day, which is conducive to aviation safety. The distribution of the average ΔV with V_M for the three visibility meters is illustrated in Figure 5b. It can be seen that the ΔV of the three instruments was negative at each V_M level. The absolute value of ΔV continuously increased with increasing V_M, and the absolute value of ΔV for LT_{23} was the largest when $V_M \leq 6403$ m, while the absolute value of ΔV for FD was the largest when $V_M > 6403$ m. In general, the value of V_I was smaller than V_M at all V_M levels, and the larger the V_M value, the greater the negative deviation. At a low V_M, LT_{23} exhibited the most significant negative deviation; at a high V_M, the negative deviation was most prominent for FD.

3.4. Distributions of the Deviation and Relative Deviation of V_I Relative to V_M

3.4.1. Overall Distribution Patterns

The ΔV of the three visibility meters mainly lay in the range of $[-2000$ m, 0 m$]$ (see Figure 6a), accounting for 69.1–71.9% of all ΔV values. Most of the data were distributed in $[-1000$ m, -500 m$)$, followed by $[-2000$ m, -1500 m$)$ and then zero-ΔV data. FD provided significantly more zero-ΔV data and more ΔV with an absolute value exceeding 2000 m compared with the two sets of LT. According to the distribution of zero-ΔV values with V_M for the three sets of visibility meters (see Figure 6b), the zero-ΔV values of FD were mainly distributed in the range of $V_M > 4017$ m. When $V_M \leq 847$ m, the zero-ΔV data of FD were significantly less than those of the two sets of LT. In addition, the distribution of ΔV with V_M in $[-500$ m, 500 m$]$ (see Figure 6b) revealed that, when $V_M \leq 847$ m, the percentage of zero-ΔV values for FD was also apparently lower than those of the two sets of LT, indicating that the two sets of LT had a closer V_I to V_M than FD at V_{M800}.

The distribution of ΔV_{Mdi} (see Figure 6c) shows that almost all (96.3–98.3%) ΔV_{Mdi} values were between $[-60\%, 60\%]$, and the proportion was the highest for LT_{05} and the lowest for v. Approximately 60% of the ΔV_{Mdi} data lay in the range of $[-40\%, 0\%)$. Based on the distribution of the proportion of ΔV_{Mdi} within $\pm 20\%$ with V_M (see Figure 6d), when $V_M \leq 847$ m, this proportion for FD was significantly lower than those of the two sets of LT, meaning that the deviation of FD's V_I relative to V_M was much greater than those of the two sets of LT at V_{M800}.

3.4.2. Distributions of Deviation and Relative Deviation at V_{M800}

Figure 7a shows that, at V_{M800}, the ΔV values of the three visibility meters were predominantly negatively deviated, accounting for more than 80% of all ΔV values, with an overall negatively skewed distribution pattern. The proportion of negatively deviated ΔV was the highest for LT_{23}, reaching 90.6%. The ΔV values were mainly in the range of $[-200$ m, 0 m$]$, accounting for 57.8–62.5%, and this proportion was the highest for LT_{23} and the lowest for FD. The ΔV of LT_{05} was mostly distributed between $[-200$ m, 200 m$]$, accounting for 71.9%, and the ΔV of LT_{23} and FD mainly lay in $[-400$ m, 0 m$]$, accounting for 75.0% and 73.4%, respectively. FD had significantly fewer zero ΔV values than the two sets of LT but significantly more absolute ΔV values exceeding 1000 m, indicating that the distribution of ΔV was negatively skewed and that the V_I of LT_{23} was generally smaller than V_M at V_{M800}. The V_I of LT_{05} was the closest to V_M, while the deviation of V_I from V_M was the greatest for FD.

At V_{M800}, the ΔV_{Mdi} of the three visibility meters mainly lay in the range of $[-100\%, 0\%]$, accounting for 81.3–90.6% of all ΔV_{Mdi} data, and this proportion was the highest for LT_{23} and the lowest for LT_{05}. In general, the ΔV_{Mdi} values were concentrated between

[−80%, −40%), accounting for 51.4–54.7%, and the overall distribution pattern was negatively skewed by 40% (see Figure 7b). Among the three sets of visibility meters, the ΔV_{Mdi} of LT_{05} was mainly distributed in [−80%, 0%], accounting for 79.7% of all its ΔV_{Mdi} data. The ΔV_{Mdi} values of LT_{23} and FD were predominantly between [−100%, −20%), accounting for 78.1% of their ΔV_{Mdi} data. FD had a significantly smaller proportion of ΔV_{Mdi} in [−20%, 20%] than the two sets of LT. Overall, the distribution of ΔV_{Mdi} was negatively skewed by 40% at V_{M800}. The deviation of V_I from V_M was the least for LT_{05} and the greatest for FD, and the extent of deviation for LT_{23} and FD was greater than that for LT_{05} by 20%.

The average (AVG), maximum (MAX), and minimum (MIN) values of ΔV and ΔV_{Mdi} for the three visibility meters at V_{M800} are listed in Table 5. In general, V_I was smaller than V_M by 70–124 m, with a relative deviation of 17.4–21.8%. The MAX of ΔV and ΔV_{Mdi} for the different instruments varied significantly, and the largest values reached 2000 m and 1000%, respectively, all corresponding to LT_{23}, which were significantly higher than those of the data of the other two visibility meters. The differences in the MIN of ΔV and ΔV_{Mdi} for the different instruments were relatively small, and the absolute values of their MIN were considerably smaller than the MAX values. Statistical analysis revealed that the MAX and MIN of ΔV and ΔV_{Mdi} for the different visibility meters appeared in March and April in spring. The MAX values occurred during fog dissipation or when dense fog turned into mild fog, that is, when visibility improved rapidly; the MIN values appeared at the beginning of the formation of fog or dense fog, that is, when visibility decreased rapidly. The reason for this may be that, as V_M improves, once the RVR of the airport meets the requirements for take-off or landing, aircrafts are allowed to take off or land. Fog on the airport runway is disturbed by the aircraft; therefore, its dissipation is faster than that in other areas. Thus, the visibility along the runway direction differs significantly from that around the airport. When V_M decreases, visibility often fluctuates slightly, and the instrumental response is more rapid and sensitive than that under manual observation.

Table 5. AVG, MAX, and MIN of ΔV and ΔV_{Mdi} when V_M < 800 m.

Statistic	LT_{05}		LT_{23}		FD	
	ΔV (m)	ΔV_{Mdi} (%)	ΔV (m)	ΔV_{Mdi} (%)	ΔV (m)	ΔV_{Mdi} (%)
AVG	−70	−17.4	−124	−21.8	−74	−21.4
MAX	1000	233.3	2000	1000.0	1300	550.0
MIN	−500	−83.3	−650	−92.9	−600	−100.0

3.5. Influence of RH on the Deviation and Relative Deviation of V_I from V_M

Several studies [33–35] have suggested that atmospheric RH substantially impacts visibility. Therefore, in this study, we statistically analysed the difference between V_I and V_M under different RH levels.

3.5.1. Influence of RH on the RMSE and RRMSE of V_I Relative to V_M

The distribution of RMSE with RH for the three visibility meters (see Figure 8a) showed that the RMSE of FD increased rapidly with RH, representing the largest increase rate among the three instruments, and the most significant increase occurred when 55% ≤ RH < 95%. The variations in RMSE with RH for the two sets of LT were relatively moderate. The RMSE of LT_{23} increased slightly overall, and the increase rate was much lower than that of FD; the RMSE of LT_{05} decreased slightly in general, with the most remarkable decline being at RH ≥ 95%. For the two sets of LT, the variation trends of their RMSE were essentially the same when RH < 75%, that is, the RMSE increased with RH at low humidity and then decreased when RH reached a certain level. The variation trends diverged when RH ≥ 75%. From this point, the RMSE of LT_{23} increased continuously with increasing RH; the RMSE of LT_{05} rapidly decreased with increasing RH, only exhibiting a slight increase when 85% ≤ RH < 95%. This may have been because LT_{23} was closer to the sea, with a distance of less than 1000 m from the seashore; thus, it was frequently affected

by sea fog. When RH < 65%, the RMSE of FD was significantly smaller than that of the two sets of LT; when RH $\geq$ 75%, the RMSE of FD was apparently larger than that of LT_{05} and comparable to that of LT_{23}.

RRMSE increased with RH for all three sets of visibility meters (see Figure 8b), and the increase was particularly prominent when RH $\geq$ 85%. The increase rate was the largest for FD, followed by LT_{23}. When RH < 75%, the RRMSE of LT was higher than that of FD; when RH $\geq$ 85%, the RRMSE of FD was higher than that of LT_{05} and comparable to that of LT_{23}.

The above analysis shows that the influence of RH on LT_{05} is relatively small, while FD is significantly affected by RH. As RH increased, the increase in ΔV and ΔV_{Mdi} for FD was more remarkable than that for LT. At low humidity, the RMSE and RRMSE of FD were smaller than those of LT. However, when RH $\geq$ 85%, these two values for FD were significantly larger than those for LT_{05} and comparable to those for LT_{23}.

3.5.2. Influence of RH on the Distributions of the Deviation and Relative Deviation of V_I from V_M

The ΔV values of LT were predominantly distributed in [−2000 m, −500 m) under each RH level, but as RH increased, the proportion of ΔV in this interval gradually decreased, and the proportion of ΔV in [−500 m, 500 m] gradually increased (see Figure 9a,b). At low humidity (RH < 45%), the ΔV of FD was evenly distributed over [−2000 m, 2000 m] (see Figure 9c). With increasing RH, the proportions of the data in [500 m, 2000 m] and [−500 m, 500 m] declined rapidly, and the proportion of ΔV lower than −2000 m continuously increased until it reached dominance when RH $\geq$ 85%. Therefore, with increasing RH, the proportion of small deviations in the FD results decreased rapidly, and that of large deviations increased rapidly. As shown by the distribution of the difference in the ΔV of LT_{05} and FD under different RH levels (see Figure 9d), when RH < 65%, the proportion of small ΔV for FD was higher than that for LT_{05}, and the proportion of large ΔV for LT_{05} was higher than that for FD; as RH increased, the pattern changed, with an increase in the proportion of small ΔV for LT_{05} and an increase in the proportion of large ΔV for FD; by RH $\geq$ 85%, the proportion of small ΔV for LT_{05} was higher than that for FD, and the proportion of large ΔV for FD was higher than that for LT_{05}. Such patterns further indicate that RH significantly affects the results for FD more than it affects those for LT.

The distribution of ΔV_{Mdi} with RH (see Figure 10a–c) showed that, with increasing RH, the proportion of ΔV_{Mdi} in [−20%, 20%] gradually decreased, and the proportion of ΔV_{Mdi} in [−80%, −20%) gradually increased for all three visibility meters. In addition, the magnitude of such decreases and increases for FD was more significant than that for the two sets of LT. When RH < 85%, the proportion of ΔV_{Mdi} in [−20%, 20%] was higher than that in [−80%, −20%) for all three instruments; when RH $\geq$ 95%, the proportion of ΔV_{Mdi} in [−80%, −20%) was higher than that in [−20%, 20%]. As revealed by the distribution of the difference in the ΔV_{Mdi} of LT_{05} and FD under different RH levels (see Figure 10d), when RH < 65%, the proportion of ΔV_{Mdi} in [−20%, 20%] for FD was significantly higher than that for LT_{05}; the proportion of ΔV_{Mdi} in [−80%, −20%) for LT_{05} was apparently higher than that for FD. As RH increased, the magnitude of such differences decreased. When RH $\geq$ 85%, the proportion of ΔV_{Mdi} in [−20%, 20%] for LT_{05} was significantly higher than that for FD, and the proportion of ΔV_{Mdi} in [−80%, −20%) for LT_{05} was significantly lower than that for FD. These findings also confirm that the influence of RH on FD was more significant than that on LT. Therefore, LT was more suitable than FD to serve as the main visibility detection equipment at airports located in high-humidity areas, which is consistent with the conclusion of Chan [36].
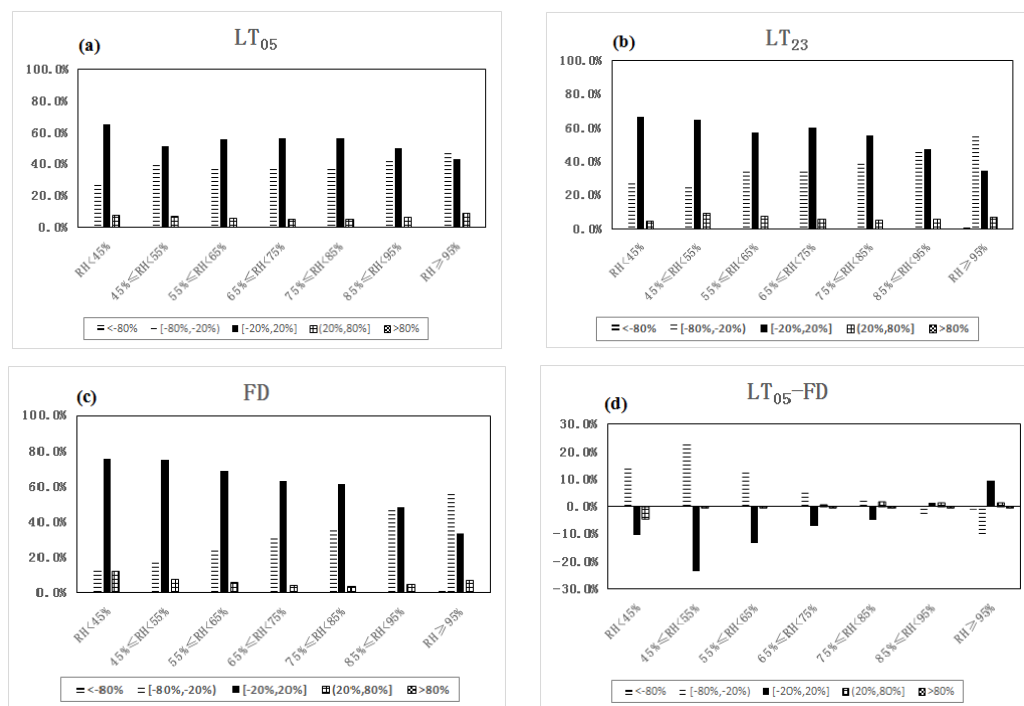
Figure 10. Proportional distributions of (**a**) $\Delta V_{Mdi, LT05}$, (**b**) $\Delta V_{Mdi, LT23}$, (**c**) $\Delta V_{Mdi, FD}$, and (**d**) $\Delta V_{Mdi, LT05-FD}$ under different RH levels from 2015 to 2020.

4. Conclusions

We obtained the following conclusions by comparing the V_I results of two sets of Vaisala transmissometers (LT_{05} and LT_{23}) and one set of forward-scatter meters (FD) with manually obtained V_M values and analysing the variation of the differences between V_I and V_M with RH.

The ΔV values of the three visibility meters were predominantly negative. In particular, the proportion of negative ΔV values accounted for more than 80% at V_{M800}, which is conducive to ensuring the safety of aviation operations.

The V_I values of LT_{05} were the closest to those of V_M. At V_{M800}, the RMSE and RRMSE of FD were higher than those of the two sets of LT, the number of zero-ΔV values for FD was significantly lower than that for LT, and the large ΔV and large ΔV_{Mdi} values of FD were much higher than those of LT. Thus, a transmissometer is the optimum visibility detection equipment among Vaisala instruments for airports along the south-eastern coast of China.

RH substantially impacted FD. When RH < 75%, the RMSE and RRMSE of FD were lower than those of the two sets of LT; as RH increased, the RMSE and RRMSE of FD increased rapidly, with a particularly significant increase in high humidity, and the large ΔV and ΔV_{Mdi} values of FD were significantly higher than those of LT. Therefore, transmissometers are more suitable visibility detection instruments than FD in high-humidity environments. The performance of FD at Xiamen Airport was restricted by the factory-calibrated physiochemical properties of aerosols, but the physiochemical properties of aerosols vary regionally, and their optical properties change significantly under the influence of environmental humidity. Thus, the detection performance of FD in high-humidity environments requires further assessment based on measurements obtained for inland and plateau areas.

Anthropogenic causes increased the difference between V_I and V_M at night. Adding target lamps can effectively reduce this difference.

References

1. *AC-97-FS-2011-01*; Guidelines on the Formulation and Implementation of the Minimum Standards for Civil Aviation Airport Operations. Civic Aviation Administration of China: Beijing, China, 2011.
2. Amalberti, R. Chapter 10: Safety in Flight Operations. In *Reliability and Safety Hazardous Work Systems: Approaches to Analysis and Design*; Wilpert, B., Qvale, T., Eds.; Lawrence Erlbaum: Hove, UK, 1993; pp. 171–194.
3. Li, H. The Understanding of Optical. *Air Traffic Manag.* **2001**, *1*, 34–36.
4. Tai, H.; Zhuang, Z.; Liu, H.; Sun, D. Automatic Observation Methods of Airport Prevailing Visibility. *Meteorol. Sci. Technol.* **2019**, *47*, 222–228.
5. Xing, X.; Cui, Y.; Zhang, F.; Xie, B. Summary of Present Situation and Development Trend of Visibility Measurement Technology. *Metrol. Meas. Technol.* **2010**, *30*, 15–20.
6. Zeng, S.; Wang, G. Observation and Instrument of Visibility. *J. Appl. Meteorol. Sci.* **1999**, *10*, 207–212.
7. Wang, W.; Zhang, S.; Zhang, C.; Fang, H.; Wang, M. Performance Analysis of Self-Developed Transmission Visibility System. *Meteorol. Sci. Technol.* **2020**, *48*, 163–170.
8. Wang, M.; Fang, H.; Zhang, S.; Wang, W.; Wang, M.; Zhu, J.; Fang, X. A Method for Testing Forward Scattering. *Meteorol. Sci. Technol.* **2021**, *49*, 12–17.
9. Mo, Y.; Liu, J.; Lu, W. Experimental Analysis of a Visibilimeter's Prototype. *Trans. Atmos. Sci.* **2004**, *27*, 230–237.
10. Li, H.; Sun, X. Theoretical Analysis on Measurement Error of Forward Scattering Visibility Meter. *Infrared Laser Eng.* **2009**, *38*, 1094–1098.
11. Xiao, S.; Huang, X.; Zhang, Z.; Qian, H.; Yang, L. The Effect of Field Angle for Forward Scattering Visibility Receiver on Measurement. *Mod. Radar* **2015**, *37*, 78–82.
12. Zhou, S.; Ma, Z. Influence of LED Surface Characteristics of Transmittance Meter on Visibility Measurement. *J. Appl. Opt.* **2016**, *37*, 719–724.
13. Wang, H.; Zu, F.; Yuan, C.; Bao, Y.; Wu, H.; Zhu, J. Comprehensive Observation Experiment and Comparative Analysis of the Forward Scattering Visibility Meter and Atmospheric Transmission Visibility Meter. *J. Meteorol. Sci.* **2022**, *42*, 225–234.
14. Ma, S.; Xu, Z.; Mao, J.; Liu, D.; Zhang, C.; Yang, L.; Zhen, X. Experimental Research on Visibility Reference Standard for Blackbody Targets. *J. Appl. Meteorol. Sci.* **2014**, *25*, 129–134.
15. Czarnecki, T.; Perlicki, K.; Wilczewski, G. Atmospheric Visibility Sensor Based on Backscattering Using Correlation Coding Method. *Opt. Quantum Electron.* **2015**, *47*, 771–778. [CrossRef]
16. Muhammad, I.; Zabih, G.; Joaquin, P.; Brazda, V.; Fiser, Q. Enhancing the Atmospheric Visibility and Fog Attenuation Using a Controlled FSO Channel. *IEEE Photonics Technol. Lett.* **2013**, *25*, 1262–1265.
17. Han, Y.; Xie, C.; Rao, R. Comparison and Analysis of Two Visibility Detecting Methods Based on Optical Scatter Technology. *Infrared Laser Eng.* **2006**, *35*, 173–176.
18. Li, X.; Quan, W.; Wang, D.; Wang, D. Comparison of Visibility Measurements Using DNQ1 and FD12 Visibility Meters and Their Major Influencing Factors. *J. Meteorol. Environ.* **2021**, *37*, 25–32.
19. Tan, H.; Chen, H.; Wu, D.; Deng, X.; Deng, T.; Li, F.; Zhao, X.; Bi, X. The Performance Evaluation and Data Correction of the Forward Scattering Visibility Sensor. *J. Trop. Meteorol.* **2010**, *26*, 687–693.
20. Zhu, L.; Li, L. Calibration Techniques for Forward Scattering Visibility Meters. *Meteorol. Sci. Technol.* **2013**, *41*, 1003–1007.
21. Yang, Y.; Hu, X. Miriam PWD20 Visibility and Comparative Analysis of Visibility and Visual. *J. Lanzhou Univ. (Nat. Sci.)* **2009**, *45*, 61–63.

22. Liu, N.; Ma, Y.; Wang, Y. Comparative Analysis of Atmospheric Visibility Data from the Middle Area of Liaoning Province Using Instrumental and Visual Observations. *Res. Environ. Sci.* **2012**, *25*, 1120–1125.

23. Xia, D.; Wu, Z.; Tan, H.; Yuan, Z.; Chen, L.; Huang, P. Analysis and Correction of Visibility Measured by Automatic Observing System in Guangdong. *Meteorol. Sci. Technol.* **2014**, *42*, 68–72.

24. Wu, H.; Huang, X.; Mo, C. Analysis of Difference between M6000 Visibility Sensor and Manual Observation Visibility. *Meteorol. Sci. Technol.* **2015**, *43*, 595–600.

25. Si, P.; Gao, R. A Comparative Evaluation on Automatic and Manual Observations of Fog and Haze in Tianjin. *J. Appl. Meteorol. Sci.* **2015**, *26*, 240–246.

26. Zhang, H.; Chen, L. Comparative analysis of visual visibility and instrumental visibility on Guangzhou airport. *J. Meteorol. Res. Appl.* **2010**, *31*, 123–125.

27. He, F.; Yuan, Y. Comparative analysis of automatic and manual visibility observation at airport meteorological station. *J. Green Sci. Technol.* **2019**, *12*, 27–29.

28. International Civil Aviation Organization. *Manual on Automatic Meteorological Observing Systems at Aerodromes*; International Civil Aviation Organization: Montreal, QC, Canada, 2013.

29. *AP-117-TM-2012-01*; Guidelines for Meteorological Station Construction at Civil Aviation Airports. Civic Aviation Administration of China: Beijing, China, 2012.

30. *AP-117-TM-2021-01R2*; Specifications for Ground-based Civil Aviation Meteorological Observations. Civic Aviation Administration of China: Beijing, China, 2021.

31. Wang, R.; Zhou, X.; Li, C. Analysis on Visibility Difference Between Manual and Automatic Observation in Jiangsu. *J. Meteorol. Sci.* **2015**, *35*, 183–188.

32. Wang, C.; Huang, Y.; Li, D.; Jiang, M.; Chen, W. Analysis of the Errors in Automatic and Manual Observations of Visibility. *J. Meteorol. Res. Appl.* **2015**, *36*, 111–112.

33. Liu, F.; Tan, Q.; Jiang, X.; Jiang, W.J.; Song, D.L. Effect of Relative Humidity on Particulate Matter Concentration and Visibility During Winter in Chengdu. *Environ. Sci.* **2018**, *39*, 1466–1471.

34. Du, R.; Qi, B.; Hu, D.; Li, L.; Yu, B. The Analysis of Relative Humidity and $PM_{2.5}$ Impact on Visibility in Hangzhou. *J. Nanjing Univ. (Nat. Sci.)* **2015**, *51*, 473–480.

35. Gong, S.; Feng, J. Relationships among Relative Humidity, PM_{10} Concentration and Atmospheric Visibility in Shanghai. *Res. Environ. Sci.* **2012**, *25*, 628–631.

36. Chan, P.W. A Test of Visibility Sensors at Hong Kong International Airport. *Weather* **2016**, *71*, 241–246. [CrossRef]